Relaxation of Self-Entangled Many-Arm Star Polymers

Gary S. Grest,*,† Kurt Kremer,‡,§ S. T. Milner,† and T. A. Witten†

Corporate Research Science Laboratory, Exxon Research and Engineering Company, Annandale, New Jersey 08801, and Institut für Physik, Universität Mainz, D-6500 Mainz, Federal Republic of Germany. *Received June 13, 1988; Revised Manuscript Received September 9, 1988*

ABSTRACT: We present a description of the relaxation of star polymers based on the conformational scaling properties predicted by Daoud and Cotton and confirmed in our recent simulations. We identify three typical relaxation mechanisms. The first describes elastic deformation of the overall shape. Its relaxation time is nearly independent of f. A second type of relaxation occurs via rotational diffusion. We predict that the relaxation time should scale with $N^{2\nu+1}f^{2-\nu}$ where ν is the correlation length exponent. A third relaxation process is the disentanglement of two or more arms. Here the longest relaxation time should increase exponentially with $f^{1/2}$. We measure various relaxation processes by molecular-dynamics simulations of star polymers with many ($6 \le f \le 50$) arms. The observed relaxation times are consistent with our predictions but do not give strong confirmation. We also discuss how the observed scaling behavior should be modified by hydrodynamic interactions, which are not treated in the simulations.

I. Introduction

Recent progress in synthesizing branched polymers has led to heightened interest[1] in their spatial and temporal statistical properties. A special class of branched polymers is the star polymer, which may be thought of as linear polymers joined at one of their ends to a common center. The diameter of the center typically is of the order of a few bond lengths but is much smaller than the extension of a polymer. Well-characterized star polymers have been synthesized with up to 18 arms connected to a single center.[2] By using linear polymers which have a small associating end group on one end only, it is possible to produce starlike structures with many more arms.[3] However, samples of this type typically have a very large polydispersity with respect to their number of arms. Most of the previous theoretical analysis[4-8] was concerned with static properties in the high molecular weight limit. These analytic predictions were partially confirmed by Monte Carlo simulations[9-13] and series expansions.[10] Recently we[14] performed a detailed analysis of the static properties of many-arm star molecules. Our molecular dynamics simulations[15] included dissipative forces and as such are sufficiently realistic to model relaxation properties of the self-entangled star as well as the static properties. In this paper we report our results for how the star relaxes.

The static properties of star polymers were analyzed by using the Daoud–Cotton scaling picture.[4,5] These authors use the blob model to describe the overall structure of such star polymers. The idea is that the density of monomers from the center decays as a power law. At a given distance r from the center, a sphere of radius r is cut by f arms. Thus depending on the distance from the central vertex, a star should look like a semidilute solution with a screening length $\xi(r)$, where $\xi(r)$ is a function of only r and the number of arms f. At a given distance r from the center, there are f blobs, one for each polymer chain. Since f blobs cover a sphere of radius r, the blob radius

$$\xi(r) \propto rf^{-1/2} \tag{1}$$

As in any semidilute solution, each blob ξ contains $n_B \propto \xi^{1/\nu}$ monomers. Here ν is the correlation length exponent, which is 0.588 for a good solvent ($d = 3$).[16] From this picture, one can easily verify that $\rho(r)$, the number density of monomers, falls off as

$$\rho(r) \propto f^{(3\nu-1)/2\nu}r^{(1-3\nu)/\nu} \qquad (=f^{0.65}r^{-1.30}) \tag{2}$$

Qualitatively, this scaling behavior is nicely illustrated by Figure 1, in which we show a projection of a typical configuration of a star polymer with $f = 10$ for $N = 50$, 100, and 200. Similar projections for $f = 30$ and 50 are shown in ref 14. It shows nicely the density falloff and corresponding increase in ξ with increasing r, as expected. For the average center end distance $\langle R^2 \rangle$ and radius of gyration of the whole star $\langle R_G^2 \rangle$, one finds

$$\langle R^2 \rangle \propto \langle R_G^2 \rangle \propto N^{2\nu}f^{1-\nu} \tag{3}$$

where N is the number of monomers per arm. In ref 14 we showed that these relations are well satisfied for f from 6–50 arms. More recently Batoulis and Kremer[12] have shown using detailed Monte Carlo simulations that even for $f = 3$, 4 these relations are well obeyed for $\langle R_G^2 \rangle$. We also compared our results for $\langle R_G^2 \rangle / \langle R_{G1}^2 \rangle$ to experimental data for polystyrene and polyisoprene stars.[17] Here $\langle R_{G1}^2 \rangle$ is the radius of gyration for a single polymer of chain length equal to one of the arms. For $3 \le f \le 18$, where experimental data are available for relatively monodisperse samples, the agreement with our simulations[14] is excellent. Thus it appears that the scaling analysis gives a good description of the static properties of stars. We may now ask how well this picture predicts the dynamic relaxation processes.

The organization of the article is as follows. In the next section we discuss the three main relaxation processes expected in a star polymer both with and without hydrodynamic interactions. There we make extensive use of the scaling picture discussed in the Introduction. Section III describes the details of the simulations. These simulations display only a subset of the expected relaxation processes. At short times the mean-squared displacements are as exected for simple linear polymers. At long times the motion appears consistent with the predicted time scale for elastic relaxation discussed in section II. In section IV we present results for the autocorrelations identified in section II. Finally, section V contains a short summary and our conclusions.

II. Relaxation Processes of Star Polymers

If we consider a star polymer with many arms f, we can think of three qualitative relaxation processes, which will occur on different time scales and will only weakly couple

† Exxon Research and Engineering Company.
‡ Universität Mainz.
§ Present address: Institut für Festkörperforschung der Kernforschungsanlage Jülich, D-5170 Jülich, Federal Republic of Germany.

0024-9297/89/2222-1904$01.50/0

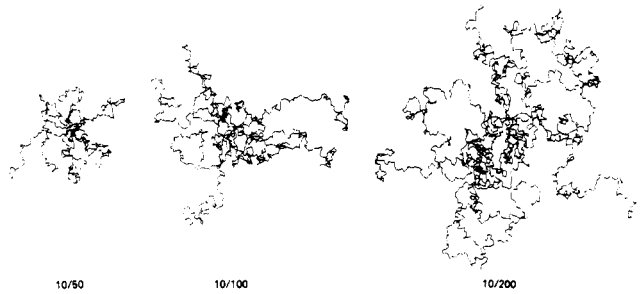

Figure 1. Projections of a typical configuration of a star of f = 10 with N = 50, 100, and 200.

to each other. Since we want to understand their principal nature, we discuss and try to analyze them separately. In principle these mechanisms also should occur for linear polymers; however, in the star polymers one is able to look at each of them separately.

First, the star relaxes via overall shape fluctuation, or elastic modes. Their time scale is that of cooperative diffusion over the star size R. We gave a short account of this process already in ref 14. A second process is rotational diffusion of the object. For a linear polymer f = 1, 2, this motion has the same relaxation time, up to a constant of order unity, as that of the elastic shape fluctuations. But for many arms f, the shape fluctuations relax progressively faster. Hence, the two time scales have the same dependence on the number of monomers per arm N but different dependence on the number of arms f. The rotational diffusion is slower since it is not enhanced by the pressure within the star, as the elastic modes are.

The third process—by far the slowest—is the disentangling of two (or more) intertwined arms. Such a configuration, *especially for many-arm stars, can easily* survive the shape or rotation relaxations. The more arms the object has, the better we will be able to distinguish these three processes.

The first detailed analysis of the dynamics of branched polymers was performed by Zimm and Kilb[18] already in 1959. They solved the Rouse[19] and the Zimm[20] model for the Zimm–Stockmayer approximation.[21] There each pair of arms is treated as an individual and independent random walk. For static properties this approximation works very well for the good solvent case[12,22] for few arms while it does not work for the Θ-regime. It should be noted that the different relaxation mechanism cannot be distinguished in this approach, since it is based on the fact that the pairs are independent and can freely penetrate. We will compare their results to ours below.

First let us consider the fastest process. The shape fluctuations controlled by the breathing or elastic modes are directly apparent in fluctuations of the inertia tensor **M**. We define **M** as the sum of the dyadic product of the distances of the positions $\mathbf{r}_{i,j}$ from the center of mass $\mathbf{r}_{cm}$ of the whole star. Here the index denotes the jth monomer on arm i. Evidently $\mathbf{r}_{cm} = [1/(Nf + 1)]\sum_{ij}\mathbf{r}_{ij}$ as usual. Then the inertia tensor $\boldsymbol{M}$ is given by

$$\boldsymbol{M} = \frac{1}{Nf+1}\sum_{j=1}^{N}\sum_{i=1}^{f}(\mathbf{r}_{ij} - \mathbf{r}_{cm})\cdot(\mathbf{r}_{ij} - \mathbf{r}_{cm}) \quad (4)$$

With this the mean-squre radius of gyration $\langle R_G^2\rangle$ can be expressed as

$$\langle R_G^2\rangle = \langle M_{xx} + M_{yy} + M_{zz}\rangle \quad (5)$$

The typical shape fluctuations now are given by the time autocorrelation function of R_G^2, the off-diagonal matrix elements of **M**, the radius of gyration R_{Ga} for each individual arm, or the squared center end distance R for each individual arm. For example, the autocorrelation function $C_R(t)$ for the end–center distance is defined by

$$C_R(t) = (\langle R(t)R(0)\rangle - \langle R\rangle^2)/(\langle R^2\rangle - \langle R\rangle^2) \quad (6)$$

How does such a fluctuation occur and relax? In ref 14 we gave a brief account based on the single-arm distance. Here we put it in a more general framework. In a semidilute solution of polymers, density fluctuations are governed by the screening length ξ. For distances larger than ξ these fluctuations decay exponentially with distance. For stars, the largest length available for such fluctuations is given by the size of the largest blob. The largest blob has a diameter

$$\xi_{max} = \xi(R) \propto Rf^{-1/2} \quad (7)$$

Typically $n_{Bmax} \propto (Rf^{-1/2})^{1/\nu}$ monomers are in such a blob. Here R is the average center–end distance of the arms. Thus, the typical shape fluctuations of a star are constructed from independent density fluctuations on the length scale of the blobs. Since the bulk of the monomers[4] are to be found in blobs of size of order ξ_{max}, density fluctuations typically occur on length scales of the order of the ξ_{max}. Thus, one also has to expect that the relative amplitude of the fluctuation of $\langle R_G^2\rangle$ and $\langle R^2\rangle$ falls off as $\xi_{max}/R \propto f^{-1/2}$. The longest relaxation time τ_B of such a local fluctuation is given by the Rouse time of an isolated chain of n_B monomers:

$$\tau_B \propto \xi_{max}^2 n_{Bmax} \propto n_{Bmax}^{1+2\nu} \quad (8a)$$

Since $n_{Bmax} \propto (Rf^{-1/2})^{1/\nu}$, this gives

$$\tau_B \propto (Nf^{-1/2})^{1+2\nu} \propto \tau_R f^{-(1+2\nu)/2} \quad (8b)$$

where τ_R is the Rouse time of an individual arm.

So far we have described the initial local relaxation. In order to produce an overall shape fluctuation, a density fluctuation has to diffuse a distance of the order of the diameter of the star polymers, which is R. The diffusion constant for a semidilute solution is given by the square of the screening length ξ divided by the local relaxation time τ_B. The relaxation rate of shape fluctuations is governed by the time such a concentration fluctuation needs in order to travel a distance R. Thus, the longest relaxation time τ_{el}, with el for elastic, is of the order of

$$\tau_{el} \propto \tau_B(R/\xi_{max})^2 \propto N^{1+2\nu}f^{1-[(1+2\nu)/2]} = N^{2.18}f^{-0.09} \quad (9)$$

For the Zimm case, with hydrodynamic interactions, the situation is slightly different. We again consider the same semidilute arrangement of blobs, however, the typical blob relaxation time $\tau_B \sim \xi_{max}^3$. For larger distances the hydrodynamic interaction is screened, so that the relation $\tau_{el} = \tau_B(R/\xi)^2$ is unaltered. Inserting this into eq 9 gives for the Zimm[20] case:

$$\tau_{el} \propto \xi_{max}^3(R/\xi_{max})^2 \propto N^{3\nu}f^{(2-3\nu)/2} = N^{3\nu}f^{+0.125} \quad (10)$$

It is perhaps more instructive to relate the Zimm time τ_{el} to the relaxation time of a linear chain with the same diameter since the Zimm time is governed by the overall volume of the polymer. Inserting eq 7 into eq 10 gives $\tau_{el} \propto R^3 f^{-1/2}$. Thus a star relaxes of order $f^{-1/2}$ faster than a linear chain of the same overall diameter.

One may distinguish two different types of elastic relaxation. One type is the global relaxation of concentration over the whole star. The other type is the relaxation of a single arm independently of the others. The former type should occur on the time scale τ_{el} as discussed above. The time scale τ_s for the latter, single-chain relaxation may be estimated by supposing the chain to be confined in a tube of radius ξ_{max}. Such a chain has an end-to-end distance of order R, and its overall dynamics are similar to that in

a Daoud–Cotton cone. In order for concentration fluctuations in this tube to relax, they must diffuse over a distance R via cooperative diffusion. Again, as with the global elastic modes, the relaxation time τ_s is of order $\tau_B R^2/\xi^2$. The independent single-chain relaxation and the many-chain elastic relaxation occur on the same time scale.

After such relaxations have occurred, the center of mass of the overall object has only moved a short distance. A much longer time is required for the whole object to rotate or to move a distance comparable to its own diameter, since the same time is needed for the star to move its own diameter or to make a complete rotation.[23] For an assembly of Nf objects subjected to independent random forces as in the Rouse model, the diffusion constant is given by

$$D \propto (Nf)^{-1} \tag{11}$$

Within the diffusion time, the system moves a distance of about its diameter. Thus the diffusion time is given by

$$\tau_D \propto R^2/D \propto NfN^{2\nu}f^{1-\nu} \propto N^{2\nu+1}f^{2-\nu} \tag{12}$$

This time still is smaller than for a linear chain of Nf monomers but much larger than the typical time of the shape fluctuations. Since the diffusion constant is very small, it is difficult to measure in a simulation. We will consider the rotational diffusion. To measure rotational diffusion, which should have a relaxation time comparable to τ_D, we can analyze the time autocorrelation function of the center–end vector $\mathbf{R}$ defined by

$$C_{RD}(t) = \langle \mathbf{R}(t)\cdot\mathbf{R}(0)\rangle / \langle R^2\rangle \tag{13}$$

where we have used $\langle \mathbf{R}(t)\rangle = 0$. Each star contains f such center–end vectors, whose autocorrelations may be averaged to improve the statistical uncertainties.

We now estimate the overall diffusion rate for the case of Zimm dynamics. Now the diffusion constant D scales with the diameter of the object; namely, $D \propto R^{-1}$. Inserting this into eq 12 gives

$$\tau_D \propto R^2/D \propto R^3 \propto N^{3\nu}f^{3(1-\nu)/2} \tag{14}$$

Again the motion is faster than for the linear chain of Nf monomers.

Even when the star moves its own distance, the topological arrangement of two arms may be largely intact. We especially think of two intertwined arms which can follow the shape fluctuations of the star without changing its topological character. We now want to describe how to simulate and calculate a relaxation process which is governed by such effects. It is important that the quantity we are looking for survives both shape fluctuations and a rotation of the whole object. It, however, should not survive a disentangling fluctuation. First let us imagine how such a disentangling process might occur.

We begin by considering the related problem of braiding entanglements in a polymer "brush" of chains in a good solvent attached by one end at moderately high coverage ρ_a (attachments per unit area) to a flat surface.[24] The conformations of such chains may be viewed as being a string of "blobs" of size $\xi \sim \rho_a^{-1/2}$, one atop the next, extending away from the grafting surface. Adopting an artificial lattice of size ξ, we would describe the conformation of a grafted chain as being a nearly straight walk away from the surface. However, because the energy required to overlay two blobs is only of order k_BT, there will be some finite fraction of "sideways steps", i.e., of subsequent blobs at the same distance from the surface.

Suppose we have S blobs in a chain and αS sideways steps on our lattice ($0 < \alpha < 1$). Then the sideways steps, taken in random directions, are a two-dimensional random walk; the free end of the chain will be displaced parallel to the surface a distance of order $\xi(\alpha S)^{1/2}$ from the grafted end.

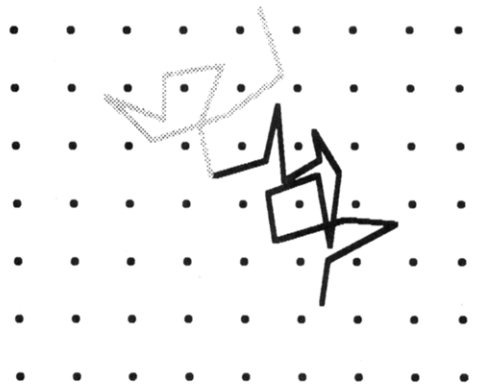

Figure 2. Two configurations of a random chain attached at one end to a horizontal plane with a lattice of vertical spikes. In one step, the chain may move one nearest-neighbor distance laterally or may move vertically upward by the same distance. In order to move from the one configuration shown to the other, the chain must pass through the completely vertical configuration.

Now consider how a chain's kinetics take it from one configuration of sideways steps to another. It suffices to view the chains with which our chain is entangled as being stationary, vertical obstacles on a regular lattice. Then, viewing from above, we have the problem of an end-attached two-dimensional random path in an entanglement network, Figure 2. The time required for the kth step from the free end to randomize its direction, denoted τ_k, is some constant c times the time required for the $(k-1)$st step and above to be free of constraint:

$$\tau_k \approx c\tau_{k-1}$$

Thus the time to observe the kth step to explore its phase space is $\tau_k \sim c^{k-1}\tau_1$, where τ_1 is the time scale during which the topmost blob may shift its position by ξ. The relaxation time grows exponentially with the number of steps k.

A similar exponentially slow relaxation should occur in the star polymer. The sideways steps made by a chain on its way out from the center are along the constant-r surfaces; the displacements of interest of the kth blob are angular displacements; each sideways step gives an angular displacement of order $f^{-1/2}$.

The time τ_1, in a Rouse dynamics simulation, is the Rouse time τ_B for a blob introduced in eq 8a above. Since ξ and thus τ_1 vary with r, we write

$$\tau_k/\tau_B(\xi(r_k)) \approx c\tau_{k-1}/\tau_B(\xi(r_{k-1})) \tag{15}$$

Now $\xi^2(r) \approx r^2/f$ and $r_k/r_{k-1} \approx 1 - f^{-1/2}$, so

$$\tau_k \approx [c(1 - f^{-1/2})^{2/\nu}]^k\tau_B \tag{16}$$

where τ_B is now the Rouse time of the largest blob. The largest time scale is the τ_k where $k \sim f^{1/2}\log N$ is the number of blobs per arm; hence the time to unbraid completely scales as

$$\tau_e \sim \exp(cf^{1/2}) \tag{17}$$

where c is a constant. This unbraiding time becomes very long as f increases. The angular displacement θ of a given chain end (for $\theta \ll \pi$) should be given by $\langle\theta^2\rangle \sim k(t)/f \sim f^{-1}\log(t/\tau_B)$.

The time over which such as entangled state survives drastically increases with the number of arms, since the surrounding arms stabilize such an entangled structure. Note that the standard knot interpretation does not work here. Although two intertwined arms do not necessarily form a mathematical knot, they still are strongly entangled.

One sensitive quantity should be the scalar product of two arbitrary center end vectors: $\mathbf{R}_i \cdot \mathbf{R}_j$, where $\mathbf{R}_i$ is the vector from the vertex to the free end of the ith arm. This dot product is largest for nearby arms; these would typically be intertwined. The product for two initially nearby arms relaxes to zero as these disentangle. To observe this quantitatively, we define the entanglement correlation function $C_e(t)$ as

$$C_e(t) = \frac{1}{f(f-1)} \sum_{\substack{i,j=1 \\ i \neq j}}^{f} \langle [\mathbf{R}_i(0)\cdot\mathbf{R}_j(0)][\mathbf{R}_i(t)\cdot\mathbf{R}_j(t)] \rangle \quad (18)$$

where we have used the fact that $\langle \mathbf{R}_i(0)\cdot\mathbf{R}_j(0) \rangle = 0$. This angular correlation may only decay after two arms which are strongly entangled have disentangled. Note that an overall rotation of the star does *not* affect $C_e(t)$, since it is a scalar. Since this correlation function is easily measurable in principle in the course of a simulation, we think that this quantity should identify the third kind of relaxation to reasonable accuracy.

At this point we should mention that the Zimm–Kilb treatment[18] leads to qualitatively different results. For the free draining (Rouse) case, the individual relaxation times of the Rouse modes yield (in our notation) $\tau_p \sim N^2/p^2$ independently of f. The sum of all relaxation rates then gives $\sum_p \tau_p \sim N^2(f-1)$. For the Zimm case the calculations yield $\sum_p \tau_p \sim N^2 f^{1/2}$, which strongly disagrees with our results. This is expected because the Zimm–Kilb analysis does not take account of the osmotic pressure inside the star due to the interactions between arms.

III. Model and Method

To test the various relaxation processes described in the previous section, we carried out a simulation of star polymers with many arms. We used a molecular dynamics method in which each monomer is coupled to a heat bath.[14] Each polymer consists of a vertex monomer which is connected with f linear arms. Each arm has N monomers, with one free end and one end attached to the vertex monomer. We refer to a star as f/N to characterize the number of arms and number of monomers per arm. The equation of motion satisfied by monomer i is given by

$$\frac{d^2\mathbf{r}_i}{dt^2} = \nabla U_i - \Gamma \frac{d\mathbf{r}_i}{dt} + \mathbf{W}_i(t) \quad (19)$$

where Γ is the bead friction which acts to couple the monomers to the heat bath and $\mathbf{W}_i(t)$ describes the random force of the heat bath acting on each monomer. $\mathbf{W}_i(t)$ is a Gaussian white noise with

$$\langle \mathbf{W}_i(t)\cdot\mathbf{W}_j(t') \rangle = \delta_{ij}\delta(t-t')6k_BT\Gamma \quad (20)$$

where the T is the temperature. Using the Einstein relation, this leads to a diffusion coefficient for an isolated bead $D_0 = k_BT/\Gamma$. Since we do not include hydrodynamic interactions in our calculations, the model is coherent with Rouse (but not with Zimm) dynamics. The potential U_i has two parts $U^0 + U^{ch}$.

$$\begin{aligned} U^0(r) &= 4\epsilon[(\sigma/r)^{12} - (\sigma/r)^6 + 1/4] \qquad r \leq r_c \\ &= 0 \qquad r > r_c \end{aligned} \quad (21)$$

is a shifted, short-range repulsive Lennard-Jones potential, which vanishes beyond a range $r_c = 2^{1/6}\sigma$ and acts between any two monomers. The potential $U^{ch}(r)$ is an attractive potential between neighboring monomers along the sequence of each arm. The parameters for this potential are the same as in ref 14. The time step was $\Delta t = 0.006\tau$, where $\tau = \sigma(m/\epsilon)^{1/2}$. Here m is the mass of each monomer. Note that Δt cannot be mapped directly onto a microscopic time scale, because a single monomer corresponds to a number of real bonds, which depend on the chemistry. The simulations were carried out for a reduced temperature $k_BT/\epsilon = 1.2$ and bead friction $\Gamma = 0.5\tau^{-1}$. Because the potential between monomers which are not chemically linked along the chain is purely repulsive, our simulations are in the good solvent regime. The average bond length between nearest-neighbor beads along the chain was found to be 0.97σ and the persistent length 1.3σ. Our choice of parameters for the attractive potential $U^{ch}(r)$ ensure that bonds do not cut each other for the reduced temperature $k_BT/\epsilon = 1.2$.[14]

Table I
Ratios of Equilibrium Dimensions of Star Polymers Defined by the Components R_{Gi}^2 of the Inertia Tensor, Equation 4[a]

f/N	M	$\langle R_{G3}^2 \rangle$	$\langle R_{G2}^2 \rangle$	$\langle R_{G1}^2 \rangle$
1/50	20000	15.07	3.05	1.00
6/50	2000	3.60	2.27	1.00
10/50	13000	2.32	1.44	1.00
20/50	5000	1.70	1.38	1.00
30/50	6500	1.67	1.31	1.00
50/50	2600	1.30	1.14	1.00
10/100	2000	2.35	1.62	1.00

[a] M is the number of configurations, taken $100\Delta t$ or 0.6τ apart, over which the data are averaged.

For a given bead friction Γ, the motion of a monomer is undamped (with the chain constraints) for $t < \Gamma^{-1}$, while for $t \gg \Gamma^{-1}$ it shows typical Rouse behavior.[19] Our choice of $\Gamma^{-1} = 2\tau$ means that the ballistic motion of a monomer is confined to about two to three bond lengths for a single chain. For larger distances the motion is diffusive. This choice was a convenient compromise. For smaller values of Γ, the coupling to the heat bath is too weak and the star samples phase space very ineffectively. It does not show the desired Rouse behavior for a single chain until very late times. For larger values of Γ, the viscosity damping and random force term dominate over the inertia term in eq 19. This means that the motion would be dominated by Langevin dynamics even for very early times and there could be little cooperative motion of the monomer; this is important for movement to occur particularly in the dense interior of the star. This limit would make the algorithm very ineffective. A more general discussion of this numerical approach is given in ref 14 and 15. This short-time ballistic region will show up for short time $t \lesssim 2 - 3\Gamma^{-1} = 4\text{–}6\tau$ in the autocorrelation and dynamic functions presented in the next section. However, since the total length of the runs are typically longer than 1000τ (see Table I), this does not cause any difficulty.

The simulation was started with the arms stretched radially and isotropically away from the center for the first 50 monomers. To the end of each arm further beads in a random-walk configuration were added to make up the required total N. Thus, the initial configuration has a larger radius of gyration than the final star, and the arms were initially well separated.

The amount of overall translational or rotational motion expected on the time scale of our simulation is small. The Rouse diffusion constant in this system is $(Nf)^{-1}$ times the diffusion constant of an individual bead. Using this, we expect a center-of-mass displacement in our 50/50 star of only a few diameters in time 2500τ. The transverse displacement of a typical bead due to rotation is expected to be of the same order.

For our systems, it is important to remember that since $f^{1/2} < N$, we do not have a very large extended core region. Therefore, we need only consider the so-called "swollen

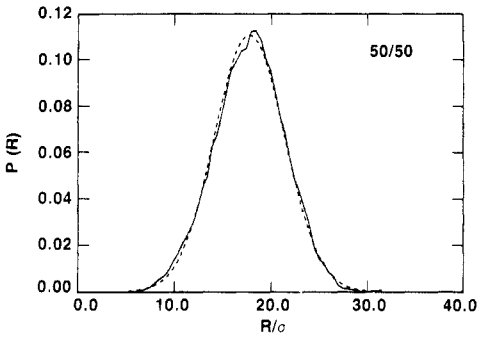

Figure 3. Distribution function $P(R)$ for the center–end distances versus R for the 50/50 star. The solid line is the raw data, while the dashed line is a Gaussian with the same width and standard deviation as the data.

regime" of Daoud–Cotton[4] and do not have to worry about their inner Θ-like or meltlike regimes. This feature shows up most strongly in our results for $\rho(r)$ which follow the scaling form, eq 2, after only one to three inner monomers.

In ref 14 we presented the results for the static properties for a number of stars. We studied systems of N = 50 bonds per arm for f = 6, 10, 20, 30, 40, and 50, as well as stars with N = 100 and 200 for f = 10. We also compared our results single chains of length 50 and 100 monomers, which we refer to as 1/50 and 2/50. Results for the mean-square end–center distance $\langle R^2 \rangle$, mean-square radius of gyration of the star $\langle R_G^2 \rangle$, and radius of gyration of each individual arm $\langle R_{Ga}^2 \rangle$ are tabulated in ref 14 for these stars. In addition, Table I presents our results for the equilibrium dimensions of our simulated star polymers defined by the components R^2_{gi} of the inertia tensor, eq 4.

To show the range of motion of the arms, we measured the distribution $P(R)$ of center–end distance R. The expected width of this distribution may be estimated from the Daoud–Cotton model,[4] by considering the center–end distance R of a chain confined in a narrow cone of opening angle $\theta = 2f^{-1/2}$. (Such a cone subtends a solid angle which is $1/f$ of the sphere.) The end–end distance of such a chain fluctuates as though is were confined in a straight tube of diameter $R\theta$. The free energy of this chain (relative to an unconfined chain) is of order $kTR/(R\theta)$, i.e., kT per blob of size $R\theta$. Decreasing the end–end distance to zero costs a further energy of this order. Thus the free energy associated with a small fluctuation ΔR of the end–end distance away from its average value $\langle R \rangle$ is of order $kTR/(R\theta)[\Delta R/R]^2$. Thus thermal fluctuations in ΔR, of energy $\simeq kT$, are expected to be of order $\langle R \rangle \theta^{1/2} = 2^{1/2}\langle R \rangle f^{-1/4}$. For many arms f we expect the distribution $P(R)$ to approach a Gaussian shape of width $\Delta R \ll \langle R \rangle$.

Another model distribution is that of polymers end grafted to a flat surface in a solvent, the "polymer brush". A recent calculation[24] shows that in this system the end–end distance R fluctuates by an amount $\Delta R \sim R$, regardless of the degree of stretching of the polymer. For the brush, $P(R)$ rises linearly for $R \ll \langle R \rangle$ and falls to zero again at a height h of order $\langle R \rangle$: $P(R) \to O((R - h)^{1/2})$. For $R > h$, $P(R)$ falls off exponentially, with characteristic width of the same order as in the cone model above.

The measured $P(R)$ is plotted in Figure 3 for f = 50. As the figure shows, the distribution is Gaussian within the uncertainly. $P(R)$ does not appear to extrapolate to zero at any particular maximal or minimal R. This is counter to the behavior of the brush[24] but consistent with the Daoud–Cotton picture.[4] The width of the $P(R)$ distribution, measured by its standard deviation, is also consistent with the Daoud–Cotton picture. As anticipated, it is

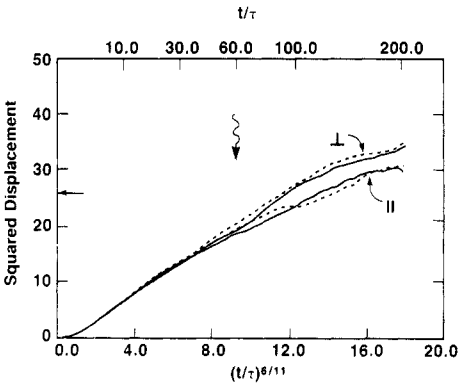

Figure 4. Mean-squared radial (∥) and transverse (⊥) displacement $(\Delta \vec{R})^2$ for the center–end distance versus time, $(t/\tau)^{6/11}$. The upper scale shows the time t/τ. The solid lines are for the 50/50 star and dashed for 20/50. The wavy arrow at $t \approx 60\tau$ indicates the relaxation time determined from the autocorrelation function for the magnitude of R; see Figure 6. The arrow at 26 on the vertical axis indicates the predicted maximum displacement for the 50/50 star, $(\Delta \vec{R})_\parallel = 2[\langle R^2 \rangle - \langle R \rangle^2]$, using the data of Figure 3.

distinctly smaller than $\langle R \rangle$ but distinctly larger than the cone width $\theta\langle R \rangle = 0.07\langle R \rangle$ defined above. It is quite comparable with the anticipated $\theta^{1/2}\langle R \rangle = 0.53\langle R \rangle$.

In addition, we measured[14] the local density $\rho(r)$ as a function of distance r from the seed monomer, as well as several static scattering functions $S(q)$. Our results were in good agreement with the asymptotic scaling predictions of the Daoud–Cotton blob model.

IV. Relaxation Phenomena

In addition to the detailed static correlations described in ref 14, our simulations can be used to give information about the relaxation dynamics of star polymers. We monitored the fluctuations in a number of quantities, including the end–center distance R, the radius of gyration of each arm R_{Ga}, and the matrix elements of the radius of gyration matrix $\mathbf{M}$ about a fixed coordinate axis. From these quantities, we can construct the autocorrelation functions defined in section II. In all cases, the average $\langle\ \rangle$ in eq 6, 13, and 18 was taken over a large number of initial states taken $20\Delta t$ apart. Results for the relaxation of $\mathbf{R}$, R, and R_{Ga} were averaged over all f arms, for $\vec{R}(t_i)\cdot\vec{R}(t_j)$ over all $f(f-1)/2$ pairs of arms and over the three off-diagonal matrix element $\mathbf{M}$.

The motion of a single arm may be conveniently monitored by using the mean-squared displacement $(\Delta \vec{R})^2 = \langle \vec{R}_i(t) - \vec{R}_i(0)^2 \rangle$ over a time t. Figure 4 compares this displacement for radial and transverse motions for the 20- and 50-arm star. At early times the motion is isotropic and $(\Delta \vec{R})^2$ increases roughly as $t^{6/11}$, as expected[15] for linear chains in solution. As the displacement ΔR reaches the mean distance $\theta R = 2f^{-1/2}R$ ($\approx$5 for 50/50 star) between chains, anisotropy appears. The transverse displacement continues to increase as for short times, but the radial displacement shows a leveling off. Asympotically this must reach a value of $2[\langle R^2 \rangle - \langle R \rangle^2]$, which we measured independently to be 26 for a 50/50 star.

To show collective motions of the ends, we have plotted the averaged transverse displacements $\Delta R_{i\perp}$ for all arms i. To form $\Delta R_{i\perp}$, we averaged the position R_i over 300τ and subtracted this from the average position for the next 300τ. This 300τ is a long time on the scale of Figure 4. The resulting displacement vectors are mapped in a Mercator projection in Figure 5. The cooperative elastic and rotational motions anticipated in section II would appear in this plot as an organized flow: nearby vectors would tend to be equal. The map shows no evidence of this cooper-

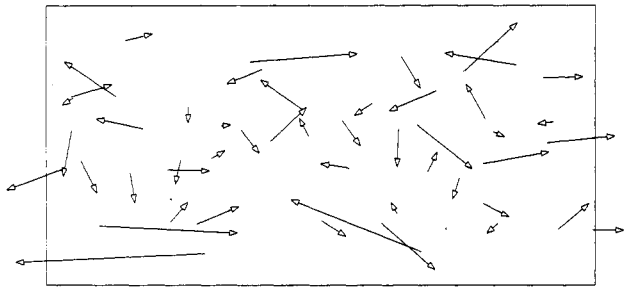

Figure 5. Mercator projection for the transverse displacement of the center–end vectors of the 50/50 star. The initial and final positions of the ends are averaged over 300τ. The duration of the simulation was over 1500τ.

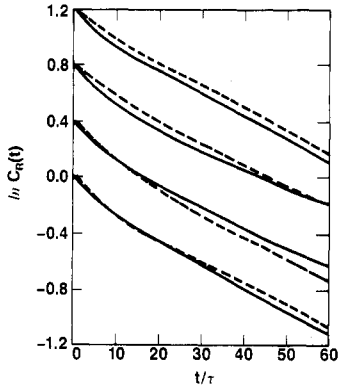

Figure 6. Autocorrelation function $C_R(\tau)$ for the end–center distance (solid lines) and single arm radius of gyration (dashed lines) for four stars of size 10/50, 20/50, 30/50, and 50/50. The curves has been displaced by 0.4 for clarity. Note that the relaxation time is essentially the same for all four.

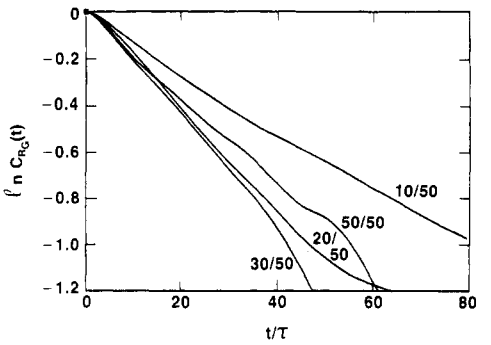

Figure 7. Autocorrelation function $C_{RG}(\tau)$ for the radius of gyration of the entire star for stars with f = 10, 20, 30, and 50 arms for N = 50. Note that the relaxation time for $f \geq 20$ is the same as that obtained for R_{Ga} and R.

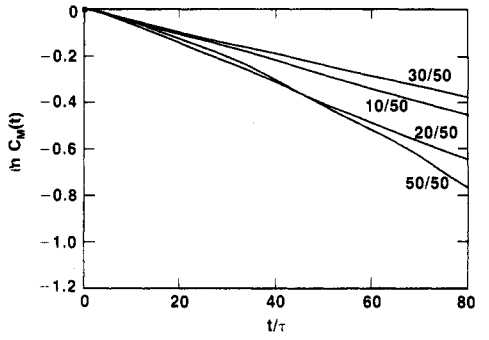

Figure 8. Autocorrelation function $C_M(\tau)$ for the off-diagonal matrix element of the radius of gyration matrix M_{xy}, M_{xz}, and M_{yz} for stars with f = 10, 20, 30, and 50 arms for N = 50. While there is no systematic dependence with f, as expected, the overall relaxation time scale is 2.5–3.5 longer than for R_{Ga} and R.

ative motion; instead, each end appears to move independently of its neighbors. The predominant motion appears to be a quasi-independent stretching and compressing of all the arms. Our measurements of the correlation functions of section II support this view.

We now consider explicitly first the relaxation of the overall shape fluctuations or elastic modes. This can be studied by using our simulations by following the decay of one of four autocorrelation functions, for end–center distance R, radius of gyration of each arm R_{Ga}, the radius of gyration of the entire star R_G, or the off-diagonal matrix elements of the radius of gyration matrix **M**. Since the latter two can be averaged over all f arms, the statistics are better but all four give basically the same results.

The observed correlation functions $C_R(t)$ for the scalar end–center distance and for the radius of gyration of a single arm are shown in Figure 6 and are consistent with the behavior predicted from the discussion in section II. The relaxation is exponential with a characteristic time $\tau_R \approx 60\tau$ for all values of f for N = 50. The results for τ_R have been tabulated in ref 14. The final relaxation time depends imperceptibly on f, as can be seen from Figure 6, and is consistent with the weak $f^{-0.09}$ dependence predicted. We determined the final relaxation time either from the slope of ln $C_R(t)$ for long time or by

$$\tau_R = \int_0^\infty C_R(t)\, dt \qquad (22)$$

Both methods gave similar results to within 10%. Since we do not measure the complete decay of $C_R(t)$, the integration was carried out numerically only from 0 to 60τ. The contribution from 60τ to infinity was added, assuming that $C_R(t)$ decayed exponentially for long times. We checked[14] the predicted N dependence for our f = 10 stars and it appeared roughly quadratic, as anticipated.

Results for $C_{RG}(t)$, the autocorrelation function for the radius of gyration of the entire star, and $C_M(t)$, the autocorrelation function for the off-diagonal elements of **M**, are shown in Figures 7 and 8, respectively. While the statistics are not as good as in Figure 6, we see that $C_{RG}(t)$ decays with the same characteristic time $\tau_R \sim 60\tau$ for $f \geq 20$. We believe the apparent slower relaxation time for f = 10 is a result of insufficient statistics. The relaxation for $C_M(t)$ shows no systematic f dependence and has a characteristic relaxation time 2.5–3.5 times longer than observed for R, R_{Ga}, and R_G. The results for both these quantities are consistent with the scaling predictions that the shape relaxation depends imperceptibly on f. These results clearly support the scaling picture compared to the independent strand approach of Zimm and Kilb[18] which predicts that $\tau \sim f$.

The next relaxation processes we considered is that of diffusion, which is predicted to scale as $\tau_D \propto f^{2-\nu}$, eq 12. However, both the translational and rotational diffusion for these large objects is very slow as discussed above and we could not measure τ_D accurately. This would require significantly longer runs than presently accessible.

The third relaxation process we consider was the disentanglement time τ_e. Figure 9 shows our results for $C_e(\tau)$, defined by eq 18 for four stars. There is clearly a strong dependence of the relaxation on the number of arms f. Unfortunately, as in the case of rotational diffusion, the decay of $C_e(\tau)$ over the total run is not sufficient to determine τ_e accurately enough to test the scaling predictions.

V. Summary

We have shown that the scaling picture for many-arm star polymers can be used to identify three typical relaxation mechanisms. For large N and f they can be studied separately. The first describes elastic deformation of the

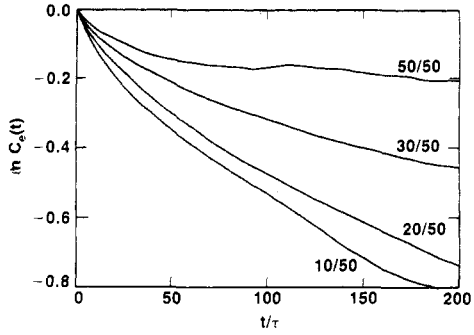

Figure 9. Entanglement autocorrelation function $C_e(\tau)$, defined by eq 18 for f = 10, 20, 30, and 50 with N = 50. Clearly τ_e has a strong dependence on f, but the decay in $C_e(\tau)$ is too slow to determine τ_e accurately.

star's overall shape and is essentially independent of the number of arms f for both the Rouse and Zimm model. The intermediate relaxation process is the translational or rotational diffusion time which scales as $N^{2\nu+1}f^{2-\nu}$ (Rouse). Both of the relaxation processes scale the same with molecular weight as for linear polymers, where shape fluctuations occur on the same time scale as translational diffusion. The third relaxation process applies only for branched polymers and describes the disentanglement of two or more arms. For a star polymer we predict that its relaxation time depends exponentially on $f^{1/2}$.

We also showed that molecular dynamics simulations of many-arm polymers with up to 50 arms can be used to study some of these expected relaxation processes. In particular, we demonstrated that the relaxation times of the center–end distance R and the mass tensor $\mathbf{M}$ depend imperceptibly on f, as expected for elastic relaxation. Further, we saw evidence for two distinct relaxation times, namely, a time $\tau_s \simeq 60\tau$ for single-arm relaxation and an overall relaxation time τ_{el} which is a factor 2.5–3.5 longer. While the other two relaxations were too slow to be measured accurately in our simulations, we did find a stronger dependence of the relaxation on the number of arms f for the disentanglement time τ_e.

The observed slowness of the entanglement process raises the question of whether our simulated stars have achieved entanglement equilibrium. As explained in section III, our star arms were initially radially stretched and hence completely unentangled. If full entanglement occurred during the equilibration, we would expect the ends to move large angular distances over the time of the simulation. This large-scale motion should be reflected in Figure 5, which shows the angular motion of all the arms over about a tenth of the total simulation time. But the actual motion shown on that figure is small; it is no more than about the angular distance between arms. This motion is not much greater than if each arm were confined in its Daoud–Cotton cone. Thus, it seems likely that the arms remain substantially disentangled throughout the simulations. This lack of entanglement may have influenced the static and dynamic properties we observed. To explore these entanglement effects—a distinctive feature of star polymers—is an important problem for future simulations.

Acknowledgment. We thank J. Batoulis, K. Binder, and P. A. Pincus for helpful discussions. K.K. acknowledges support from SFB41. G.S.G. and K.K. acknowledge support from NATO Travel Grant 86/680.

References and Notes

(1) Burchard, W. *Adv. Polym. Sci.* **1983**, *48*, 1. This paper gives an extensive review of the scattering properties of branched polymers and gives a rather complete list of references. More recent experimental papers for stars area: Roovers, J.; Hadjichristidis, N.; Fetters, L. J. *Macromolecules* **1983**, *16*, 214. Huber, K.; Burchard, W.; Fetters, L. J. *Macromolecules* **1984**, *17*, 541. Xuexin, C.; Zhongde, X.; von Meerwall, E.; Seung, N.; Hadjichristidis, N.; Fetters, L. J. *Macromolecules* **1984**, *17*, 1343. Richter, D.; Stuhn, B.; Ewen, B.; Nerger, D. *Phys. Rev. Lett.* **1987**, *58*, 2462.
(2) Dozier, W.; Huang, J.; Fetters, L. J., to be submitted for publication.
(3) Davidson, N. S.; Fetters, L. J.; Funk, W. G.; Graessley, W. W.; Hadjichristidis, N. *Macromolecules* **1988**, *21*, 112. Fetters, L. J.; Graessley, W. W.; Hadjichristidis, N.; Kiss, A. D.; Pearson, D. S.; Younghouse, L. B. *Macromolecules* **1988**, *21*, 1644.
(4) Daoud, M.; Cotton, J. P. *J. Phys. (Les Ulis, Fr.)* **1982**, *43*, 531.
(5) A slightly different ansatz than in ref 4 is used, but the same results are found: Birshtein, T. M.; Zhulina, E. B. *Polymer* **1984**, *25*, 1453; Birschtein, T. M.; Zhulina, E. B.; Borisov, O. V. *Polymer* **1986**, *27*, 1078.
(6) Miyake, A.; Freed, K. F. *Macromolecules* **1983**, *16*, 1228; **1984**, *17*, 678.
(7) Douglas, J. F.; Freed, K. F. *Macromolecules* **1984**, *17*, 1854.
(8) Vlahos, C. H.; Kosmas, M. K. *Polymer* **1984**, *25*, 1607.
(9) Mazur, J.; McCrackin, F. *Macromolecules* **1977**, *10*, 326.
(10) Lipson, J. E. G.; Whittington, S. G.; Wilkinson, M. K.; Martin, J. L.; Gaunt, D. S. *J. Phys. A: Math. Gen.* **1985**, *18*, 1469. Wilkinson, M. K.; Gaunt, D. S.; Lipson, J. E. G.; Whittington, S. G. *J. Phys. A: Math. Gen.* **1986**, *19*, 789.
(11) Freire, J. J.; Pla, J.; Rey, A.; Prats, R. *Macromolecules* **1986**, *19*, 452.
(12) Batoulis, J.; Kremer, K. *Macromolecules*, in press.
(13) Huber, K.; Burchard, W.; Bantle, S.; Fetters, L. J. *Polymer* **1987**, *28*, 1990; *Ibid* **28**, 1997.
(14) Grest, G. S.; Kremer, K.; Witten, T. A. *Macromolecules* **1987**, *20*, 1376.
(15) Grest, G. S.; Kremer, K. *Phys. Rev. A.* **1986**, *33*, 3628.
(16) LeGuillou, J. C.; Zinn-Justin, J. *Phys. Rev. B: Condens. Matter* **1980**, *21*, 3976. In the present paper we use ν = 0.59.
(17) Khasat, N.; Pennisi, R. W.; Hadjichristidis, N.; Fetters, L. J. *Macromolecules* **1988**, *21*, 1100.
(18) Zimm, B. H.; Kilb, R. W. *J. Polym. Sci.* **1959**, *37*, 19.
(19) Rouse, P. E. *J. Chem. Phys.* **1953**, *2*, 1273. de Gennes, P.-G. *Scaling Concepts in Polymer Physics*; Cornell University Press: Ithaca, NY, 1979.
(20) Zimm, B. H. *J. Chem. Phys.* **1956**, *24*, 269.
(21) Zimm, B. H.; Stockmayer, W. H. *J. Chem. Phys.* **1949**, *17*, 1301.
(22) Barrett, A. J.; Tremain, D. L. *Macromolecules* **1987**, *20*, 1687.
(23) Yamakawa, H. *Modern Theory of Polymer Solutions*; Harper and Row: New York, 1970.
(24) Milner, S. T.; Witten, T. A.; Cates, M. *Europhys. Lett.* **1988**, *5*, 413; *Macromolecules* **1988**, *21*, 2610.